ACS APPLIED MATERIALS & INTERFACES

Research Article

Cite This: ACS Appl. Mater. Interfaces 2019, 11, 10059−10067

www.acsami.org

Grinding Synthesis of $APbX_3$ (A = MA, FA, Cs; X = Cl, Br, I) Perovskite Nanocrystals

Daqin Chen,*[†,‡,§,∥] Junni Li,[‡] Xiao Chen,[‡] Jiangkun Chen,[†,§,∥] and Jiasong Zhong[‡]

[†]Fujian Provincial Key Laboratory of Quantum Manipulation and New Energy Materials, College of Physics and Energy, Fujian Normal University, Fuzhou 350117, China

[‡]College of Materials & Environmental Engineering, Hangzhou Dianzi University, Hangzhou, Zhejiang 310018, P. R. China

[§]Fujian Provincial Engineering Technology Research Center of Solar Energy Conversion and Energy Storage, Fuzhou 350117, China

[∥]Fujian Provincial Collaborative Innovation Center for Optoelectronic Semiconductors and Efficient Devices, Xiamen 361005, China

Supporting Information

ABSTRACT: Currently, metal halide perovskite nanocrystals have been extensively explored due to their unique optoelectronic properties and wide application prospects. In the present work, a facile grinding method is developed to prepare whole-family $APbX_3$ (A = MA, FA, and Cs; X = Cl, Br, and I) perovskite nanocrystals. This strategy alleviates the harsh synthesis conditions of precursor dissolution, atmosphere protection, and high temperature. Impressively, the as-prepared perovskite nanocrystals are evidenced to have halogen-rich surfaces and yield visible full-spectral emissions with maximal photoluminescence quantum yield up to 92% and excellent stability. Additionally, the grinding method can be extended to synthesize widely concerned Mn^{2+}-doped $CsPbCl_3$ nanocrystals with dual-modal emissions of both excitons and dopants. As a proof-of-concept experiment, the present perovskite nanocrystals are demonstrated to be applicable as blue/green/red color converters in UV-excitable white-light-emitting diodes.

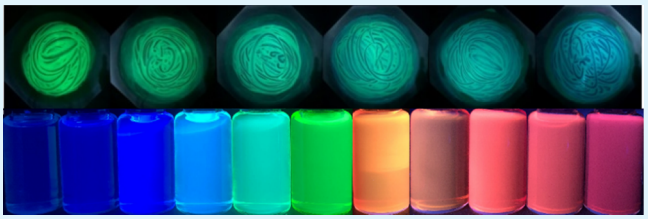

KEYWORDS: *perovskite, $CsPbBr_3$, optical materials, luminescence, LED*

INTRODUCTION

Recently, metal halide semiconductor nanocrystals (NCs) or quantum dots (QDs) with perovskite crystal structures, showing superior optical performance of narrow full width at half maximum (FWHM, down to 12 nm), high photoluminescence quantum yield (PLQY, up to 90%), and wide color gamut, have attracted intensive attention for promising applications in displays, lasers, and photodetectors.[1−16] Currently, $APbX_3$ perovskite NCs (PNCs), where A is $CH_3NH_3^+$ (MA), $CH(NH_2)_2$ (FA^+), or Cs and X is Cl^-, Br^-, or I^-,[17−27] are widely explored, and several synthesizing strategies have been developed. In 2014, Pérez-Prieto et al. reported the preparation of 6 nm sized hybrid organic-inorganic $MAPbBr_3$ PNCs for the first time by using ammonium bromide with a medium-sized chain that enables PNCs to disperse in a wide range of organic solvents.[28] Subsequently, Zhong et al. and Zeng et al. developed a ligand assisted supersaturated recrystallization method to fabricate $MAPbX_3$ and $CsPbX_3$ PNCs, respectively,[17,18] and later Levchuk et al. synthesized $FAPbX_3$ PNCs through a similar approach.[19] Importantly, a widely used synthetic route called hot injection was concurrently developed by Protesescu et al.[1] Since then, emulsion synthesis, solvothermal synthesis, microfluidic synthesis, and so on[29−34] have also been reported to prepare $APbX_3$ PNCs.

Notably, the abovementioned approaches belong to the so-called bottom-up strategy, and the monodisperse $APbX_3$ colloidal PNCs are produced via nucleation/growth of precursor ions in solution. Considering the soft feature of metal halide perovskites and their facile crystallization, a top-down strategy might also be applied to fabricate $APbX_3$ PNCs. For the top-down synthesis, external forces or energies were generally exerted on bulk materials to reduce the particle sizes into the nanoscale. Recently, solvent-free ball-milling synthesis was demonstrated to be applicable for preparing $APbX_3$ bulk powders.[35,36] Interestingly, Protesescu et al. reported a facile mechanochemical synthesis of $CsPbBr_3$ and $FAPbBr_3$ PNCs using a commercial ball mill,[37] which involved simple mechanical grinding of bulk perovskite materials in the presence of mesitylene and oleylammonium halide. Unfortunately, the usage of specific solvent and complex ligand limited the universal synthesis. For instance, compositional modifica-

Received: October 30, 2018
Accepted: February 21, 2019
Published: February 21, 2019

DOI: 10.1021/acsami.8b19002
ACS Appl. Mater. Interfaces 2019, 11, 10059−10067

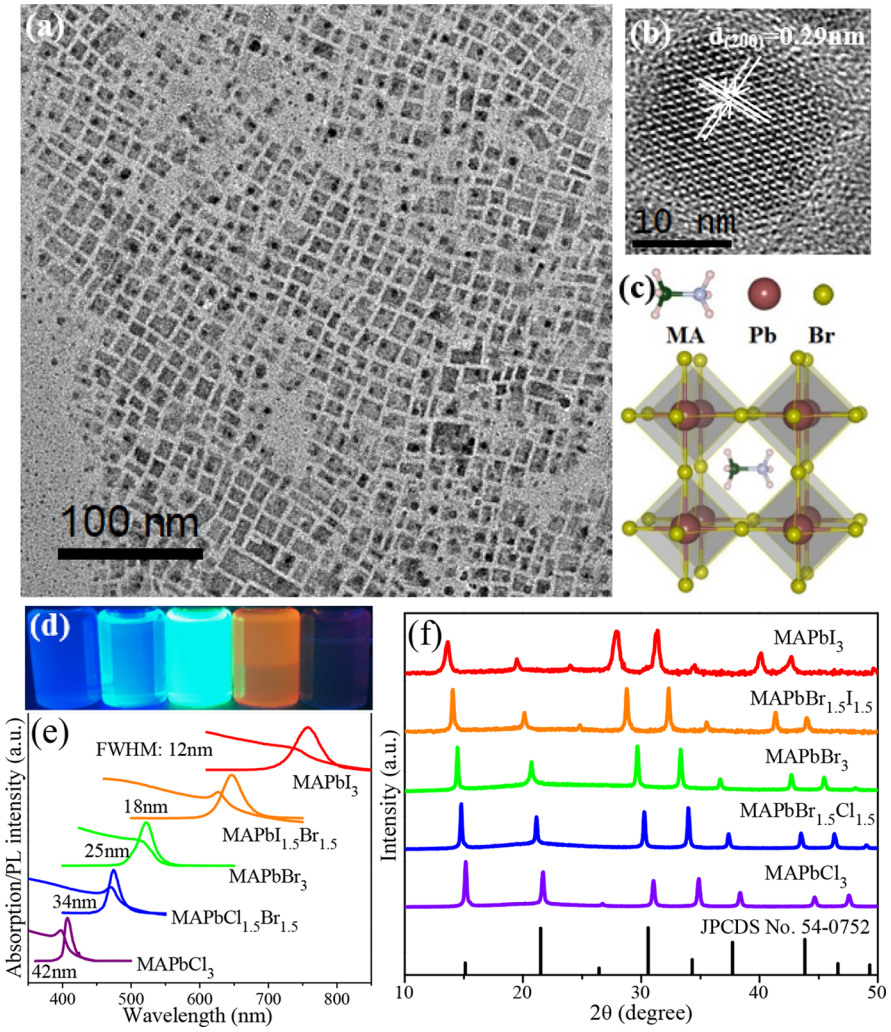

Figure 1. Monodisperse $MAPbX_3$ PNCs and their structural and optical characterizations. (a) Typical TEM and (b) HRTEM images of $MAPbBr_3$ PNCs. (c) Schematic illustration of cubic $MAPbBr_3$ perovskite structure. (d) Representative luminescence photographs of $MAPbX_3$ PNCs solutions under irradiation of 365 nm UV lamp and (e) the corresponding absorption/PL spectra. (f) XRD patterns of typical ternary and mixed-halide $MAPbX_3$ PNCs.

tion of PNC band gaps by milling bulk CsPbBr3 and oleylammonium iodide was not successful so far.

Herein, we develop a universal manual grinding method to prepare whole-family $MAPbX_3$, $FAPbX_3$, and $CsPbX_3$ PNCs for the first time. Impressively, this strategy does not require dissolving AX and PbX_2 precursors in the solvent and can be operated in an open atmosphere and at room temperature. The procedure is quite simple, that is, putting raw materials into a mortar with cyclohexane, oleic acid (OA), and oleylamine (OM) and manually grinding for a certain duration with a pestle to obtain the products. The versatility of this synthesis approach is demonstrated by fabricating different kinds of perovskite nanoparticles. The brightly emitting $APbX_3$ PNCs exhibit a high PLQY up to 92%, and the visible luminescence originating from exciton recombination can be regulated from 400 to 780 nm via modifying halogen components in PNCs. Moreover, it is interestingly found that this strategy can be extended to realize the substitution of Pb^{2+} ions by specific dopants, such as Mn^{2+} ions.

EXPERIMENTAL SECTION

Materials and Chemicals. Lead halides (PbX_2, 99.99%; Aladdin), cesium halides (CsX, 99%; Macklin), methylammonium halide (MAX, 99.5%; Xi'an Polymer Light Technology), formamidinium halide (FAX, 99.5%; Xi'an Polymer Light Technology), cesium acetate (CsOAc, 99%; Macklin), formamidine acetate (FAOAc, 99%; Macklin), OA (90%; Aldrich), OM (80–90%; Aldrich), cyclohexane (99.7%, Macklin), dimethyl sulfoxide (DMSO, 99.8%, Macklin), and poly(methyl methacrylate) (PMMA, Macklin) were used as received.

Grinding Synthesis of $APbX_3$ PNCs. Taking $MAPbX_3$ as a typical example, PbX_2 (0.2 mmol) and MAX (0.16 mmol) powders were put into an agate mortar, and 2 mL of cyclohexane was added. After grinding for 20 min to mix these powders well, OA (150 μL) and OM (30 μL) were introduced and then continued to grind for 100 min. Because cyclohexane is volatile, it was continuously added during grinding. After completion of grinding, the product was dispersed in 4 mL of cyclohexane and further purified by appropriate centrifugation. In the purification process, the original sample needs to be centrifuged three times. First, the product was centrifuged at a speed of 2000 rpm for 5 min, and the sediment was discarded. Second, the supernatant was centrifuged again at 5000 rpm for 5 min, and the sediment was discarded. Finally, the supernatant was centrifuged at 12000 rpm for 5 min, and the precipitation was the target product. The obtained $MAPbX_3$ PNCs were redispersed in

DOI: 10.1021/acsami.8b19002
ACS Appl. Mater. Interfaces 2019, 11, 10059–10067

cyclohexane for further usage. The synthesis of $FAPbX_3$ PNCs and $CsPbX_3$ PNCs is similar to that of $MAPbX_3$ ones. The only difference is that MAX was replaced by FAX or CsX as the precursor.

Grinding Synthesis of Mn^{2+}-Doped $CsPbCl_3$ PNCs. The synthesis of Mn^{2+}-doped $CsPbCl_3$ PNCs is similar to that of $CsPbX_3$ ones. The only difference is that extra $MnCl_2$ (0.08 mmol) was added in raw materials during grinding and the amount of $PbCl_2$ was changed to 0.16 mmol to assure that Cs:Pb:Mn was 2:2:1.

Supersaturated Recrystallization Synthesis of $FAPbX_3$ PNCs. First, the precursor was prepared by dissolving PbX_2 (0.2 mmol) and FAX (0.2 mmol) in DMSO (5 mL). After complete dissolution, OA (100 μL) and OM (50 μL) were added to stabilize the precursor solution. Then, 0.1 mL of the precursor solution was quickly introduced into the toluene solution (5 mL) to induce supersaturated crystallization of PNCs with vigorous stirring. Bright green emission was immediately observed after the injection.

Synthesis of PNCs Dispersed in PMMA Film. 1g of PMMA was dissolved in 10 mL of toluene at 80 °C and cooled down to room temperature to form stock solution (100 mg/mL). Afterward, 1 mL of stock solution was mixed with 1 mL of PNC (prepared by grinding for 2 h) solution in toluene (10 mg/mL) and dropwise casted on the cleaned glass substrate followed by drying in vacuum. Notably, the blue, green, and red PNC films were prepared by dispersing $MAPbCl_{1.5}Br_{1.5}$, $MAPbBr_3$, and $MAPbBr_2I$ PNCs in PMMA, respectively.

Construction of PNC-Based White-Light-Emitting Diode (WLED). As a proof-of-concept experiment, a WLED device was directly fabricated by coupling the UV chip with the as-prepared PNC films in the order of red layer, green one, and blue one. Opaque silica gels were filled around the edges of the LED to avoid the leakage of UV light.

Characterizations. X-ray diffraction (XRD) patterns of the as-prepared $APbX_3$ PNCs were recorded using a powder diffractometer (MiniFlex600 RIGAKU) with Cu Kα radiation (λ = 0.154 nm). Transmission electron microscope (TEM) observation was performed on a JEOL JEM-2010 operated at 200 kV accelerating voltage. The surface states of $MAPbBr_3$ PNCs were examined by X-ray photoelectron spectroscopy (XPS) using a VG Scientific ESCALAB MkII spectrometer. Ar^+ etching on $MAPbBr_3$ PNCs for 5 s each time was carried out to obtain the Br/Pb ratio at different depths. Absorption, PL spectra, and PLQY data for the $APbX_3$ PNCs were recorded on an Edinburgh Instruments (EI) FS5 spectrometer equipped with a continuous (150 W) xenon lamp and a 15 cm integrating sphere. Time-resolved PL spectra for exciton recombination of PNCs were detected on a fluorescence lifetime spectrometer (EI, LifeSpec-II) based on a time correlated single photon counting technique under the excitation of 375 nm picosecond laser. The average decay lifetimes were evaluated via the equation of $\tau = \int I(t)dt/I_0$, where $I(t)$ is the time-related emission intensity and I_0 is the peak intensity. Electroluminescence (EL) spectra of the constructed devices were recorded in a HAAS-2000 spectroradiometer (Everfine) under the forward bias of 20 mA. All the experiments were carried out at room temperature.

RESULTS AND DISCUSSION

The grinding synthesis of $APbX_3$ PNCs is accomplished by simply grinding the mixture of the AX and PbX_2 powders with long-chain organic ligands (OA and OM) and cyclohexane for a certain duration. Purification of PNCs is realized via elaborately controlling separation procedures for the as-prepared products (Experimental Section). Notably, the as-prepared products will be unstable without the addition of OA and OM, indicating that appropriate amounts of ligands are necessary for the present grinding synthesis. A typical TEM image of the obtained $MAPbBr_3$ PNCs shows that they are cubic-shaped and monodispersed with sizes of 10−25 nm (Figure 1a). A high-resolution TEM (HRTEM) micrograph of an individual $MAPbBr_3$ particle (Figure 1b) verifies its single-crystalline nature with high crystallinity and well-resolved lattice fringes. A typical lattice spacing of 2.9 Å, corresponding to the (200) plane of the cubic perovskite phase, is clearly observed (Figure 1b). The microstructure of the cubic phase of $MAPbBr_3$ PNCs is based on a three-dimensional network of the corner-shared $PbBr_6^{4-}$ octahedra linked by Br^- ions, where each Pb^{2+} ion coordinates with six Br^- ions and interstitial MA^+ cations are located in the cages of $PbBr_6^{4-}$ octahedra (Figure 1c).[15,24,38,39] The PL spectrum of $MAPbBr_3$ PNCs shows a narrow emission band centered at 522 nm, and the corresponding absorption spectrum exhibits a typical exciton absorption peak at 526 nm, suggesting that the luminescence of the obtained product originates from direct exciton recombination. In fact, the emission spectra of $MAPbX_3$ can be tuned over the entire visible spectral region of 400−780 nm by adjusting halide compositions in raw materials. As demonstrated in Figure 1d, multicolor luminescence of $MAPbX_3$ (X = Cl, Br, I and their mixture) colloidal particles in cyclohexane is clearly observed under irradiation of a 365 nm UV lamp. Gradual shift of emission peak and exciton absorption toward long wavelengths are distinctly detected (Figure 1e). Importantly, the narrow and single peak emission and the steep and single absorption indicate the dispersions only contain pure $MAPbX_3$ PNCs without defects. XRD patterns of $MAPbX_3$ PNCs are well coincident with those of the cubic $CsPbBr_3$ phase (JPCDS No. 75-0412). Varying the halogen element and content in $MAPbX_3$ can induce a gradual shift of diffraction peaks but will not alter the cubic structure of $MAPbX_3$ PNCs (Figure 1f). Interestingly, halogen anion exchange can be also achieved by grinding the as-prepared $MAPbX_3$ PNCs with the extra introduction of PbX_2 (X = Cl, I), which is beneficial to regulate emissive color more precisely and conveniently (Figure S1).

FWHM values of different $MAPbX_3$ (X = Cl, Cl/Br, Br, Br/I, I) PNCs were determined and are given in Figure 1e and Table S1. Apparently, the emission bandwidth of $MAPbX_3$ increases from 12 to 42 nm by changing X from Cl to I, which is probably attributed to size-induced inhomogeneous broadening. According to theoretical calculations by Protesescu et al.,[1] Bohr exciton diameters for $CsPbCl_3$, $CsPbBr_3$, and $CsPbI_3$ are 5, 7, and 12 nm, respectively, and the variation trend of Bohr exciton diameters for $MAPbX_3$ is similar. Generally, the emission wavelength will not be altered when the sizes of PNCs are larger than the Bohr exciton diameter; however, a blue shift will occur when the sizes are smaller than the Bohr exciton diameter. Therefore, as X changes from Cl to I, the size-induced inhomogeneous broadening will become more significant for long-wavelength emission, leading to a gradual increase of FWHM. The X-dependent emission intensities for different $MAPbX_3$ PNCs are provided in Figure S2a. PL intensity significantly increases when X changes from Cl to Br and then slightly decreases with further alteration from Br to I. As a supplement, PLQYs for these $MAPbX_3$ PNCs were also determined and are tabulated in Table S1, showing a similar variation trend to emission intensity. Time-resolved PL spectra of $MAPbX_3$ (X = Cl, Br, I) PNCs exhibit a gradual increase in average decay lifetime (2−94 ns) as the composition changes from $MAPbCl_3$ to $MAPbI_3$ (Figure S2b, Table S1). The inverse correlation between halide-controlled band gap and decay lifetime has been well demonstrated in $APbX_3$ (A = MA, Cs, FA) PNCs previously prepared by other methods.[1,19,40] The observed trend in decay lifetime is attributed to intrinsic optical properties of halide perovskites, where the overlap

DOI: 10.1021/acsami.8b19002
ACS Appl. Mater. Interfaces 2019, 11, 10059−10067

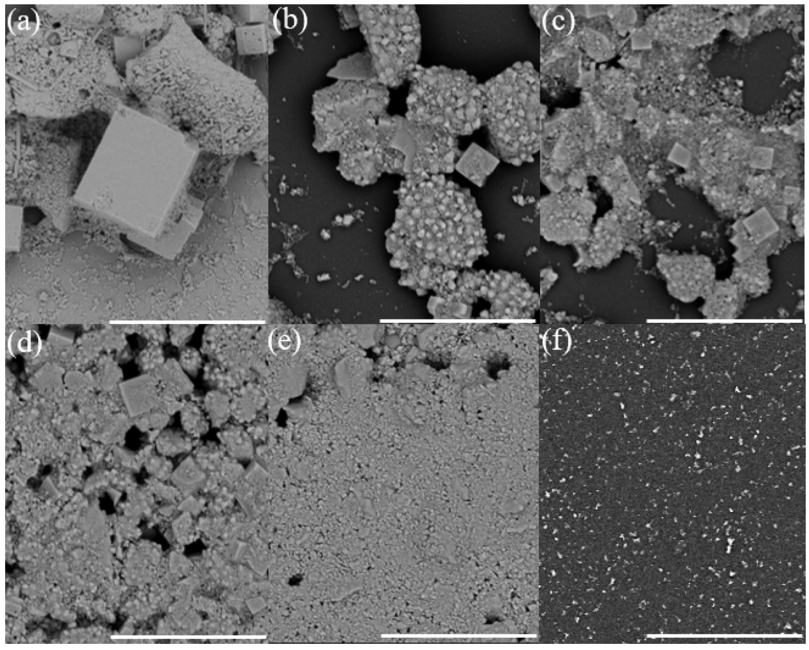

Figure 2. SEM images of $MAPbBr_3$ particles (without purification) prepared by grinding for different durations: (a) 10 min, (b) 30 min, (c) 1 h, (d) 2 h, and (e) 4 h. (f) SEM image of $MAPbBr_3$ PNCs obtained by grinding for 2 h and elaborated centrifugation treatment. All scale bars are 2 μm.

between the electron and hole wave functions will be reduced and the nonadiabatic charge-phonon coupling will be weakened with the substitution of Cl by heavy Br or Br by heavier I.[41]

To trace the evolution of morphology and size of $MAPbBr_3$ during grinding, SEM observation on the samples prepared by grinding for 10 min, 30 min, 1 h, 2 h, and 4 h (without centrifugation) was performed. It is evidenced that elongation of grinding duration can gradually reduce the size of cubic-shaped particles into the nanoscale and make them more uniform (Figure 2a–e). A SEM image of the $MAPbBr_3$ sample (2 h) after elaborated centrifugation treatment in low magnification (Figure 2f) confirms that the product after purification is indeed nanoparticles with a uniform size distribution. TEM images of $CsPbCl_3$ and $CsPbI_3$ products (Figure S2c,d) clearly demonstrate that the particle sizes are in the range of 10–25 nm. It is seriously worthy to ponder about the mechanism to synthesize metal halide PNCs by such simple grinding. Herein, taking bromide as an example shown in Figure 3, we propose that the mixture of cubic MABr and orthorhombic $PbBr_2$ (XRD data are presented in Figure S3a,b) will spontaneously and rapidly induce the formation of $MAPbBr_3$ perovskite microcrystals and further grinding will break the bulk phase into smaller nanoparticles. As shown in Figure S3c, luminescence of perovskite quickly occurs after a simple mixing of MABr and $PbBr_2$ for 5–10 s. After grinding for 10 min, the obtained product is pure cubic $MAPbBr_3$ phase even without addition of any other solvents (Figure S3d), indicating easy occurrence of chemical reaction between MABr and $PbBr_2$ to produce $MAPbBr_3$.[42,43] As we all know, halogen anion exchange in $APbX_3$ is easily realized to obtain anion hybrid perovskite such as $APb(Cl/Br)_3$ and $APb(Br/I)_3$.[44] In the present work, a single emission band was observed for the as-prepared $MAPbX_3$ (X = Cl/Br, Br/I) hybrid perovskites (Figure 1e), confirming that two kinds of halogen ions are homogeneously distributed in perovskites prepared by grinding. This gives us a hint that the cations should experience the same process, that is, homogenization of MA and Pb ions followed by the conversion of the anorthic Pb polyhedron into the cubic one (Figure 3a), where the exerting manual grind is believed to be the driving force. Further grinding will break the perovskites into nanoparticles, and elongation of grinding time will get smaller and more homogeneous PNCs (Figure 3b). Since surfactants (OA and OM) were introduced in the grinding process, they were well attached on the new interface when the bulk phase was cut into smaller particles (Figure 3b), enabling them to well disperse in nonpolar solvents such as cyclohexane (Figure 1d). As demonstrated in Figure 3c, the product became yellow after grinding and can yield bright and uniform green luminescence under the irradiation of the UV lamp.

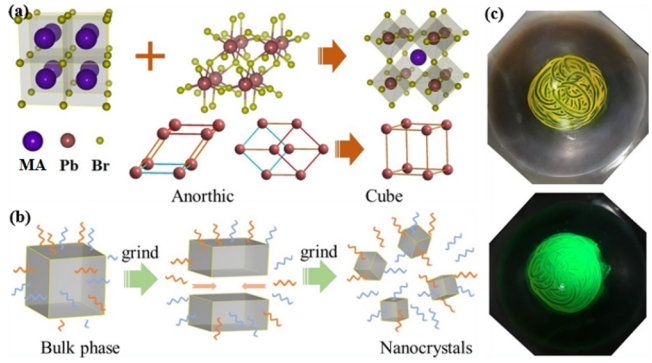

Figure 3. Schematic illustration of the formation processes of $MAPbBr_3$ PNCs by grinding: (a) chemical reaction between MABr and $PbBr_2$ to produce $MAPbBr_3$ bulk phase and (b) conversion from bulk particles into NCs with the assistance of grinding force. (c) Photographs of the product prepared by grinding for 2 h under daylight and UV lamp irradiation.

Furthermore, the influence of grinding time on optical properties of $MAPbBr_3$ PNCs was investigated. As shown in

DOI: 10.1021/acsami.8b19002
ACS Appl. Mater. Interfaces 2019, 11, 10059–10067

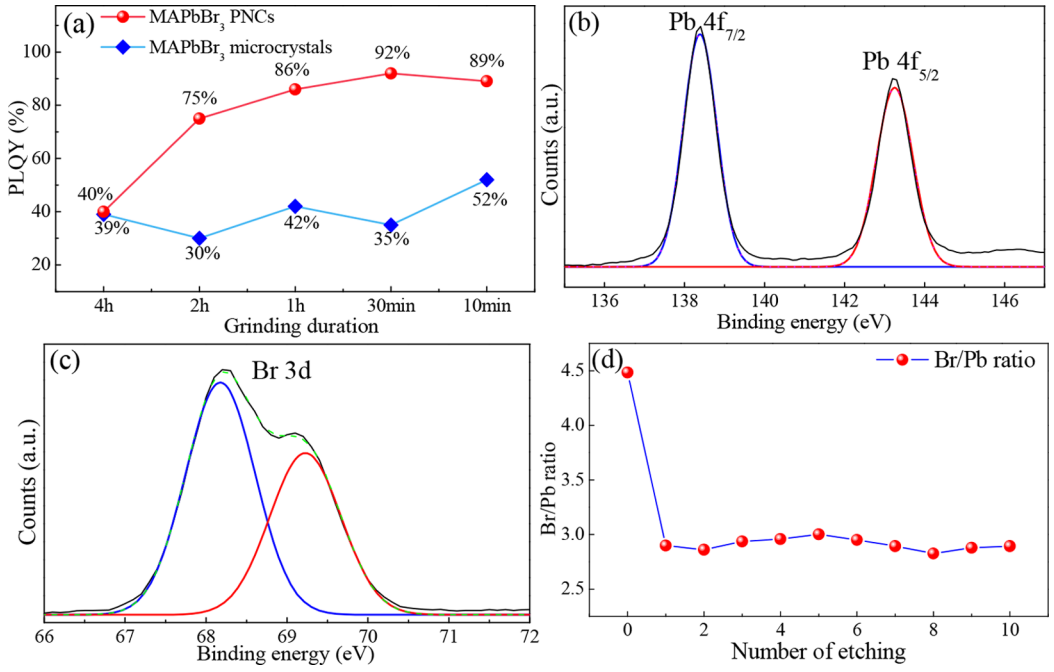

Figure 4. (a) Absolute PLQY values versus grinding time for $MAPbBr_3$ PNCs (after purification) and microcrystals (obtained from sediment). High-resolution XPS spectra of (b) Pb 4f and (c) Br 3d for the $MAPbBr_3$ PNCs. (d) Br/Pb ratio versus number of etching by Ar^+ ions.

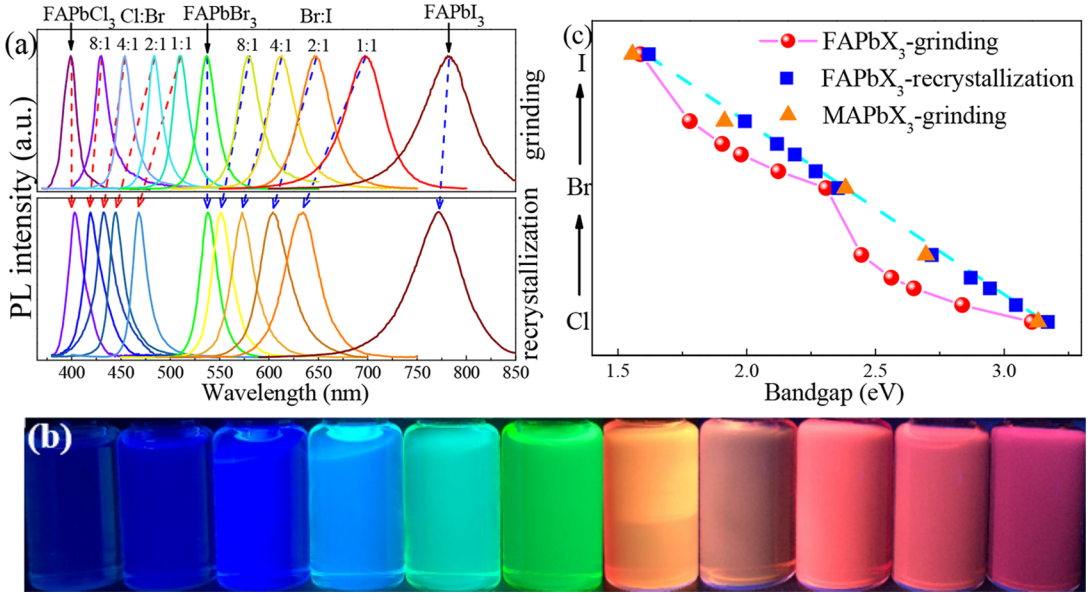

Figure 5. (a) PL spectra of $FAPbX_3$ PNCs prepared by grinding method and supersaturated recrystallization route. (b) Corresponding luminescence photographs of $FAPbX_3$ PNCs under irradiation of UV (365 nm) lamp. (c) Variation of band gaps versus halogen component in the $FAPbX_3$ ($MAPbX_3$) PNCs prepared by the grinding method and $FAPbX_3$ PNCs prepared by supersaturated recrystallization route.

Figures S4 and S5, all the samples prepared with different grinding times are pure cubic phase. Importantly, it is found that grinding time has no obvious effect on the spectral profile and position (Figure S6), indicating that the target product can be produced in an extremely short time (10 min). As shown in Figure 4a and Figure S7a, high PLQYs up to 75−92% are obtained for the as-prepared $MAPbBr_3$ PNCs via grinding for 10−120 min. However, the value tends to drop with the increase of grinding time. As a comparison, the variation of PLQYs for $MAPbBr_3$ sediments (microcrystals) obtained after centrifugation is also given in Figure 4a, showing lower PLQYs than those for the corresponding PNCs. Herein, PLQYs were employed to characterize the stability of PNCs since the product will easily decompose after exposing in air. Figure S7b shows dependence of PLQY values on exposing time in air for the $MAPbBr_3$ PNCs prepared by grinding for 30 min and the corresponding bulk materials (microcrystals). Apparently, PLQYs of $MAPbBr_3$ PNCs are always higher than those of bulk materials (Figure S7b). After exposing in air for 30 days, about 60% of PLQY of $MAPbBr_3$ PNCs can be remained while that of bulk materials is lowered down to 5% after 7 days, indicating that the stability of $MAPbBr_3$ PNCs is better than that of bulk ones. Previously, Zhong et al. demonstrated that the coordination of solvents played an important role in

DOI: 10.1021/acsami.8b19002
ACS Appl. Mater. Interfaces 2019, 11, 10059−10067

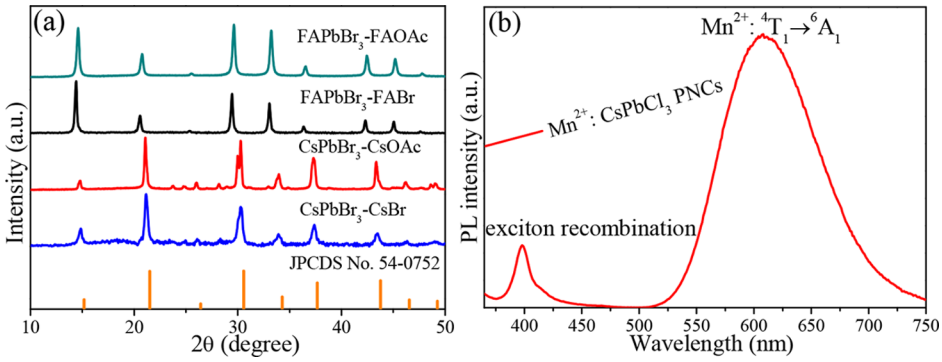

Figure 6. (a) XRD patterns of the as-prepared $FAPbBr_3$ and $CsPbBr_3$ PNCs by using FAOAc, FABr, CsOAc, and CsBr as the precursors, respectively. (b) PL spectrum of Mn^{2+}-doped $CsPbCl_3$ PNCs prepared by grinding method.

determining the stability of iodide perovskites.[45] In the present work, only cyclohexane was used as the solvent to assist manual grinding and no experiment concerning the role of different solvents on stability was carried out, which may be investigated in our further work.

XPS characterizations for the $MAPbBr_3$ PNCs (Figure S8, Figure 4b–d) were carried out to investigate their surface states. Typical Pb 4f and Br 3d signals are detected (Figure 4b,c). Specifically, the Br 3d signal can be fitted into two peaks at binding energies of 68 and 69 eV (Figure 4c), which are attributed to the inner and surface Br ions, respectively.[17,18] To further confirm this, Pb 4f and Br 4d XPS spectra of $MAPbBr_3$ PNCs upon Ar^+ etching 10 times were recorded. As evidenced in Figure 4d, the original $MAPbBr_3$ PNCs show the Br-rich surface with a Br/Pb ratio of 4.5 and after etching by Ar^+ ions, the Br/Pb ratio is close to 3 (Figure 4d). Therefore, it is concluded that the high PLQY and superior stability for the present $MAPbBr_3$ PNCs are probably attributed to the self-passivating effect of the Br-rich surface, which has been previously demonstrated in all-inorganic $CsPbBr_3$ QDs prepared by the supersaturated recrystallization route.[17]

Notably, an interesting phenomenon was observed when we intended to prepare $FAPbX_3$ PNCs (Figure S9), where the related spectroscopic data were not coincident with what we expected. Herein, all the $FAPbX_3$ (X = Cl/Br, Br/I) PNCs prepared by the grinding method were achieved by grinding the different Cl-to-Br or Br-to-I precursors for the same duration of 2 h. For instance, $FAPbBr_{1.5}Cl_{1.5}$ PNCs was previously reported to yield blue emission at ~465 nm.[3,38] However, the product prepared by the grinding method exhibited green emission at 511 nm (Figure 5a), indicating that Br^- ions rather than Cl^- ones are dominant in FA-based halogen hybrid PNCs. Actually, the same issue occurred when we synthesized $FAPbBr_{1.5}I_{1.5}$ PNCs, which showed I^- dominant red emission (Figure 5a). For better comparison, using the same precursors and halogen ratios, a series of $FAPbX_3$ (X = Cl, Br, I, Cl/Br, Br/I) PNCs were also prepared by a supersaturated recrystallization route. As revealed in Figure 5a,b, both samples show typical multicolor emissions in the visible full-spectral region, but the emission peak positions (in units of nm) of $FAPbX_3$ (X = Cl/Br, Br/I) PNCs prepared by the grinding method are located in longer wavelengths relative to the corresponding samples fabricated by the recrystallization route. As shown in Figure 5c, the band gap experiences a linear variation for the $FAPbX_3$ PNCs with an increase of Cl/Br and Br/I ratios prepared by the recrystallization route, which follows Vegard's law for lattice constants of alloys. Similarly, the band gap variation of $MAPbX_3$ PNCs fabricated by the grinding method also follows this rule. However, the experimental results of $FAPbX_3$ PNCs obtained from grinding synthesis obviously deviate from the linear shift (Figure 5c); that is, the $FAPb(Cl/Br)_3$ PNCs show Br-preferred emissions and the $FAPb(Br/I)_3$ PNCs exhibit I-leading emissions, suggesting that larger anions prefer to incorporate into FA-base PNCs during grinding. To get more information about the exact mechanism, we traced the variation of luminescence at different stages of grinding, as shown in Figure S10a. Taking the Cl/Br ratio of 4:1 as a typical example, it was found that the green emission emerged at the beginning of grinding and the luminescence gradually turned to blue with elongation of grinding time. This result confirms that the Br-dominant $FAPbBr_3$ is firstly formed upon grinding and major Cl ions enter into the crystal lattice via subsequent anion exchange (Figure S10b). A similar situation can be found for the $FAPb(Br/I)_3$ PNCs with a Br/I ratio of 4:1 (Figure S11). In fact, a geometric parameter called tolerance factor is generally required to be close to 1to maintain structural stability of $APbX_3$, where R_A and R_B are the ionic radii of the A- and Pb-site cations, respectively, and R_X is the halogen ionic radius. Considering the larger cation radius of FA (R_A = 0.21 nm) relative to that of MA (R_A = 0.19 nm), it is beneficial to stabilize the perovskite structure by incorporating larger halogen anions into the $FAPbX_3$ PNCs.

To demonstrate the generality of the grinding method, we further extend the synthesis scope to the $CsPbX_3$ PNC system. The PL color of $CsPbX_3$ varies from blue to green and finally to red as the precursor halide composition changes from Cl to Br and finally to I (Figure S12), confirming the successful grinding synthesis of $CsPbX_3$ PNCs. Interestingly, XRD results show that the as-prepared $CsPbCl_3$, $CsPb(Cl/Br)_3$, and $CsPbBr_3$ PNCs crystallize in the cubic phase structure while the $CsPb(Br/I)_3$ and $CsPbI_3$ PNCs are orthorhombic (Figure S13). Notably, one-step synthesis of orthorhombic $CsPbI_3$ PNCs was rarely reported previously and most results showed that the cubic structured $CsPbI_3$ was generally produced first and then gradually transformed into the orthorhombic one.[46−48] Finally, FAOAc and CsOAc instead of FABr and CsBr, respectively, were adopted to synthesize PNCs. XRD patterns (Figure 6a), and PL spectra (Figure S14) evidenced that different sources of A-site ions could be applied in the grinding synthesis. In fact, the $(Cs/FA)PbBr_3$ hybrid PNCs can be also prepared by this grinding method, as evidenced in Figure S15. Besides A-site ions and halogen ions, we also put sight in the B-site ions. As shown in Figure S16, Mn^{2+}-doped

DOI: 10.1021/acsami.8b19002
ACS Appl. Mater. Interfaces 2019, 11, 10059−10067

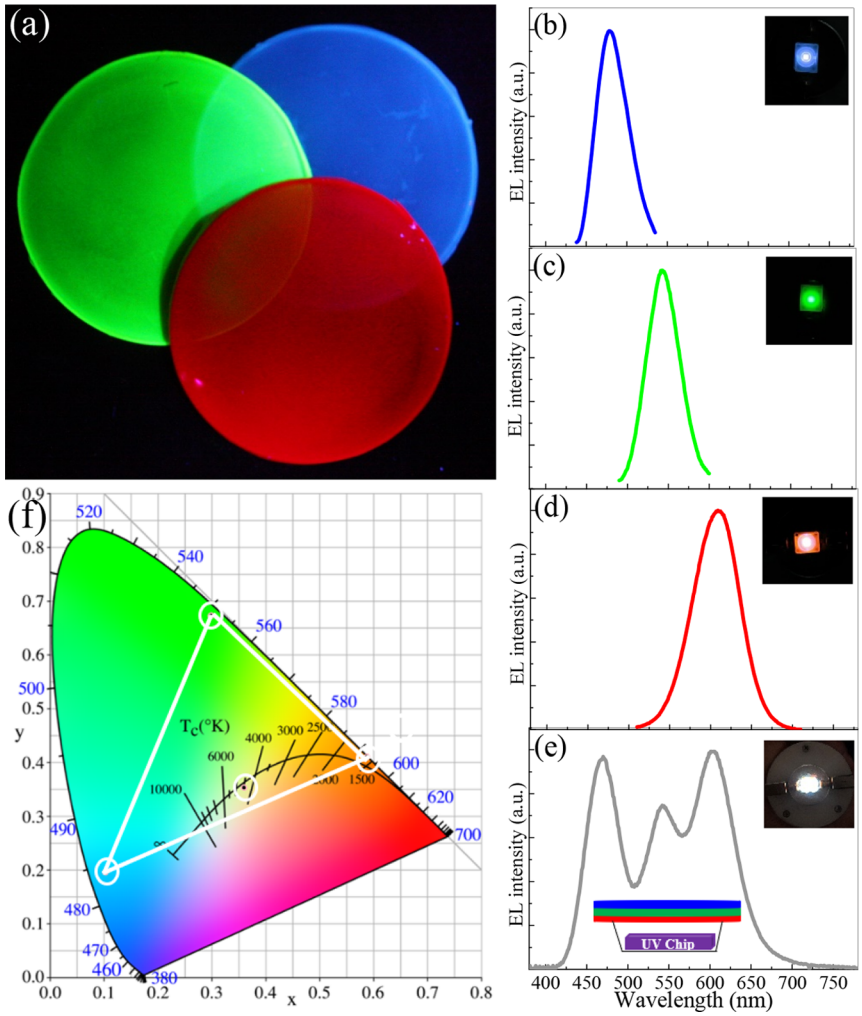

Figure 7. (a) Luminescence photographs of blue-emitting, green-emitting, and red-emitting $MAPbX_3$ PNCs dispersed in PMMA films. (b–e) EL spectra of LED devices constructed by coupling blue, green, and red PNC films and their combination with UV chip. The inset of panel (e) is the schematic illustration of a prototype LED device, and the insets of panels (b–e) are the corresponding devices driven by 20 mA operation current. (f) CIE chromaticity coordinates of the LED devices in operation.

$CsPbCl_3$ PNCs can be successfully fabricated by the grinding method after introducing an extra Mn^{2+} source (such as $MnCl_2$) into the precursors. Besides sharp violet exciton recombination emission of $CsPbCl_3$, broadband red luminescence assigned to the $^4T_1 \rightarrow {}^6A_1$ transition of Mn^{2+} was also detected (Figure 6b). Additionally, a Mn^{2+} decay curve was recorded (Figure S17). Evidently, the evaluated Mn^{2+} decay lifetime of 1.2 ms is close to the value previously reported,[49,50] verifying the feasibility of incorporating Mn^{2+} dopants into the $CsPbCl_3$ crystalline lattice by the grinding method.

Finally, we demonstrate the possible application of the present $MAPbX_3$ PNCs prepared by the grinding method as color converters in solid-state-lighting. As illustrated in Figure 7a, the $MAPbCl_{1.5}Br_{1.5}$, $MAPbBr_3$, and $MAPbI_3$ PNCs dispersed in PMMA yield three primary colors of blue, green, and red, respectively, under UV lamp irradiation. As a proof-of-concept experiment, LED devices were constructed by coupling blue $MAPbCl_{1.5}Br_{1.5}$, green $MAPbBr_3$, and red $MAPbBr_2I$ emitting films as color converters with a UV chip. EL spectra show a blue emission band originating from $MAPbCl_{1.5}Br_{1.5}$ PNCs, a green one assigned to $MAPbBr_3$ PNCs, and an orange one attributed to $MAPbBr_2I$ PNCs (Figure 7b–d). The proper adjustment of the thicknesses of blue, green, and red PNC films (2, 1, and 1.5 mm, respectively) can lead to bright white-light luminescence for the constructed LED device with a color rendering index (CRI) of 85, correlated color temperature (CCT) of 4460 K, luminous efficiency (LE) of 15 lm/W, and color coordinates of (0.360, 0.354) (Figure 7e,f). Compared to the previously reported values,[18,51−53] the optoelectronic performance for the fabricated WLED, especially LE, should be further optimized by improving PLQYs of blue- and red-emitting perovskite components. The related efforts are currently on the way.

CONCLUSIONS

In summary, we have developed a novel type of colloidal synthesis for the whole-family $MAPbX_3$, $FAPbX_3$, and $CsPbX_3$ (X = Cl, Br, I and their mixtures) PNCs with multicolor tunable emissions via a simple grinding strategy, which can be operated at room temperature and in an open atmosphere. Grinding duration evolved experiments evidenced that the mixture of AX and PbX_2 would spontaneously and rapidly induce the formation of $APbBr_3$ perovskite microcrystals and further grinding was beneficial to break the bulk phase into nanoparticles with sizes of 10–25 nm. Taking $MAPbBr_3$ as a typical sample, XPS data confirmed its Br-rich surfaces,

DOI: 10.1021/acsami.8b19002
ACS Appl. Mater. Interfaces 2019, 11, 10059−10067

enabling to achieve high PLQY up to 92% and superior stability. Impressively, Mn^{2+} dopants were demonstrated to be able to incorporate into the $CsPbCl_3$ crystalline lattice by this grinding method to produce both sharp violet exciton emission of PNCs and broadband orange emission of Mn^{2+} activators. As a result, a prototype LED device was constructed by employing the as-fabricated blue/green/red PNC films as color converters, producing bright white-light luminescence with excellent optoelectronic properties. It is believed that the present work will provide an effective route to easily synthesize perovskite nanoparticles with novel optical properties and even fabricate other low-Pb or Pb-free perovskite materials.

■ ASSOCIATED CONTENT

Supporting Information

The Supporting Information is available free of charge on the ACS Publications website at DOI: 10.1021/acsami.8b19002.

Extra absorption/PL spectra, time-resolved luminescence spectra, XRD patterns, SEM images XPS data, and luminescence photographs (PDF)

■ AUTHOR INFORMATION

Corresponding Author

*E-mail: dqchen@fjnu.edu.cn.

ORCID

Daqin Chen: 0000-0003-0088-2480

Notes

The authors declare no competing financial interest.

■ ACKNOWLEDGMENTS

This research was supported by the National Key Research and Development Program of China (2018YFB0406704), the National Natural Science Foundation of China (51572065), and the Zhejiang Provincial Natural Science Foundation of China (LR15E020001).

■ REFERENCES

(1) Protesescu, L.; Yakunin, S.; Bodnarchuk, M. I.; Krieg, F.; Caputo, R.; Hendon, C. H.; Yang, R. X.; Walsh, A.; Kovalenko, M. V. Nanocrystals of Cesium Lead Halide Perovskites ($CsPbX_3$, X = Cl, Br, and I): Novel Optoelectronic Materials Showing Bright Emission with Wide Color Gamut. *Nano Lett.* **2015**, *15*, 3692−3696.

(2) Swarnkar, A.; Chulliyil, R.; Ravi, V. K.; Irfanullah, M.; Chowdhury, A.; Nag, A. Colloidal $CsPbBr_3$ Perovskite Nanocrystals: Luminescence beyond Traditional Quantum Dots. *Angew. Chem. Int. Ed.* **2015**, *54*, 15424−15428.

(3) Protesescu, L.; Yakunin, S.; Bodnarchuk, M. I.; Bertolotti, F.; Masciocchi, N.; Guagliardi, A.; Kovalenko, M. V. Monodisperse Formamidinium Lead Bromide Nanocrystals with Bright and Stable Green Photoluminescence. *J. Am. Chem. Soc.* **2016**, *138*, 14202−14205.

(4) Kovalenko, M. V.; Protesescu, L.; Bodnarchuk, M. I. Properties and Potential Optoelectronic Applications of Lead Halide Perovskite Nanocrystals. *Science* **2017**, *358*, 745−750.

(5) Song, J.; Li, J.; Xu, L.; Li, J.; Zhang, F.; Han, B.; Shan, Q.; Zeng, H. Room-Temperature Triple-Ligand Surface Engineering Synergistically Boosts Ink Stability, Recombination Dynamics, and Charge Injection toward EQE-11.6% Perovskite QLEDs. *Adv. Mater.* **2018**, *30*, 1800764.

(6) Kovalenko, M. V.; Manna, L.; Cabot, A.; Hens, Z.; Talapin, D. V.; Kagan, C. R.; Klimov, V. I.; Rogach, A. L.; Reiss, P.; Milliron, D. J.; Guyot-Sionnnest, P.; Konstantatos, G.; Parak, W. J.; Hyeon, T.; Korgel, B. A.; Murray, C. B.; Heiss, W. Prospects of Nanoscience with Nanocrystals. *ACS Nano* **2015**, *9*, 1012−1057.

(7) Yuan, S.; Chen, D.; Li, X.; Zhong, J.; Xu, X. In Situ Crystallization Synthesis of $CsPbBr_3$ Perovskite Quantum Dot-Embedded Glasses with Improved Stability for Solid-State Lighting and Random Upconverted Lasing. *ACS Appl. Mater. Interfaces* **2018**, *10*, 18918−18926.

(8) Li, X.; Zhang, K.; Li, J.; Chen, J.; Wu, Y.; Liu, K.; Song, J.; Zeng, H. Heterogeneous Nucleation toward Polar-Solvent-Free, Fast, and One-Pot Synthesis of Highly Uniform Perovskite Quantum Dots for Wider Color Gamut Display. *Adv. Mater. Interfaces* **2018**, *5*, 1800010.

(9) Yoon, H. C.; Kang, H.; Lee, S.; Oh, J. H.; Yang, H.; Do, Y. R. Study of Perovskite QD Down-Converted LEDs and Six-Color White LEDs for Future Displays with Excellent Color Performance. *ACS Appl. Mater. Interfaces* **2016**, *8*, 18189−18200.

(10) Chung, H.; Jung, S. I.; Kim, H. J.; Cha, W.; Sim, E.; Kim, D.; Koh, W.-K.; Kim, J. Composition-Dependent Hot Carrier Relaxation Dynamics in Cesium Lead Halide ($CsPbX_3$, X=Br and I) Perovskite Nanocrystals. *Angew. Chem. Int. Ed.* **2017**, *56*, 4160−4164.

(11) Dou, L.; Wong, A. B.; Yu, Y.; Lai, M.; Kornienko, N.; Eaton, S. W.; Fu, A.; Bischak, C. G.; Ma, J.; Ding, T.; Ginsberg, N. S.; Wang, L.-W.; Alivisatos, A. P.; Yang, P. Atomically Thin Two-Dimensional Organic-inorganic Hybrid Perovskites. *Science* **2015**, *349*, 1518−1521.

(12) Quan, L. N.; García de Arquer, F. P.; Sabatini, R. P.; Sargent, E. H. Perovskites for Light Emission. *Adv. Mater.* **2018**, *30*, 1801996.

(13) Huang, J.; Lai, M.; Lin, J.; Yang, P. Rich Chemistry in Inorganic Halide Perovskite Nanostructures. *Adv. Mater.* **2018**, *30*, 1802856.

(14) Wang, Y.; Li, X.; Zhao, X.; Xiao, L.; Zeng, H.; Sun, H. Nonlinear Absorption and Low-Threshold Multiphoton Pumped Stimulated Emission from All-Inorganic Perovskite Nanocrystals. *Nano Lett.* **2016**, *16*, 448−453.

(15) Jung, H. S.; Park, N. G. Perovskite Solar Cells: from Materials to Devices. *Small* **2015**, *11*, 10−25.

(16) Chiba, T.; Hoshi, K.; Pu, Y.-J.; Takeda, Y.; Hayashi, Y.; Ohisa, S.; Kawata, S.; Kido, J. High-Efficiency Perovskite Quantum-Dot Light-Emitting Devices by Effective Washing Process and Interfacial Energy Level Alignment. *ACS Appl. Mater. Interfaces* **2017**, *9*, 18054−18060.

(17) Li, X.; Wu, Y.; Zhang, S.; Cai, B.; Gu, Y.; Song, J.; Zeng, H. $CsPbX_3$ Quantum Dots for Lighting and Displays: Room-Temperature Synthesis, Photoluminescence Superiorities, Underlying Origins and White Light-Emitting Diodes. *Adv. Funct. Mater.* **2016**, *26*, 2435−2445.

(18) Zhang, F.; Zhong, H.; Chen, C.; Wu, X.-g.; Hu, X.; Huang, H.; Han, J.; Zou, B.; Dong, Y. Brightly Luminescent and Color-Tunable Colloidal $CH_3NH_3PbX_3$ (X = Br, I, Cl) Quantum Dots: Potential Alternatives for Display Technology. *ACS Nano* **2015**, *9*, 4533−4542.

(19) Levchuk, I.; Osvet, A.; Tang, X.; Brandl, M.; Perea, J. D.; Hoegl, F.; Matt, G. J.; Hock, R.; Batentschuk, M.; Brabec, C. J. Brightly Luminescent and Color-Tunable Formamidinium Lead Halide Perovskite $FAPbX_3$ (X = Cl, Br, I) Colloidal Nanocrystals. *Nano Lett.* **2017**, *17*, 2765−2770.

(20) Xuan, T.; Yang, X.; Lou, S.; Huang, J.; Liu, Y.; Yu, J.; Li, H.; Wong, K.-L.; Wang, C.; Wang, J. Highly Stable $CsPbBr_3$ Quantum Dots Coated with Alkyl Phosphate for White Light-Emitting Diodes. *Nanoscale* **2017**, *9*, 15286−15290.

(21) Bertolotti, F.; Protesescu, L.; Kovalenko, M. V.; Yakunin, S.; Cervellino, A.; Billinge, S. J. L.; Terban, M. W.; Pedersen, J. S.; Masciocchi, N.; Guagliardi, A. Coherent Nanotwins and Dynamic Disorder in Cesium Lead Halide Perovskite Nanocrystals. *ACS Nano* **2017**, *11*, 3819−3831.

(22) Liu, F.; Zhang, Y.; Ding, C.; Kobayashi, S.; Izuishi, T.; Nakazawa, N.; Toyoda, T.; Ohta, T.; Hayase, S.; Minemoto, T.; Yoshino, K.; Dai, S.; Shen, Q. Highly Luminescent Phase-Stable $CsPbI_3$ Perovskite Quantum Dots Achieving Near 100% Absolute Photoluminescence Quantum Yield. *ACS Nano* **2017**, *11*, 10373−10383.

(23) Begum, R.; Parida, M. R.; Abdelhady, A. L.; Murali, B.; Alyami, N. M.; Ahmed, G. H.; Hedhili, M. N.; Bakr, O. M.; Mohammed, O. F. Engineering Interfacial Charge Transfer in $CsPbBr_3$ Perovskite

Nanocrystals by Heterovalent Doping. *J. Am. Chem. Soc.* **2017**, *139*, 731−737.
(24) Bekenstein, Y.; Koscher, B. A.; Eaton, S. W.; Yang, P.; Alivisatos, A. P. Highly Luminescent Colloidal Nanoplates of Perovskite Cesium Lead Halide and Their Oriented Assemblies. *J. Am. Chem. Soc.* **2015**, *137*, 16008−16011.
(25) Sun, Q.; Wang, Y. A.; Li, L. S.; Wang, D.; Zhu, T.; Xu, J.; Yang, C.; Li, Y. Bright, Multicoloured Light-Emitting Diodes Based on Quantum Dots. *Nat. Photonics* **2007**, *1*, 717−722. Yang, T.; Zheng, Y.; Du, Z.; Liu, W.; Yang, Z.; Gao, F.; Wang, L.; Chou, K.-C.; Hou, X.; Yang, W. Superior Photodetectors Based on All-Inorganic Perovskite $CsPbI_3$ Nanorods with Ultrafast Response and High Stability. *ACS Nano* **2018**, *12*, 1611−1617.
(26) Meng, L.; Yao, E.-P.; Hong, Z.; Chen, H.; Sun, P.; Yang, Z.; Li, G.; Yang, Y. Pure Formamidinium-Based Perovskite Light-Emitting Diodes with High Efficiency and Low Driving Voltage. *Adv. Mater.* **2016**, *29*, 1603826.
(27) Zhang, D.; Yang, Y.; Bekenstein, Y.; Yu, Y.; Gibson, N. A.; Wong, A. B.; Eaton, S.W.; Kornienko, N.; Kong, Q.; Lai, M.; Alivisatos, A. P.; Leone, S. R.; Yang, P. Synthesis of Composition Tunable and Highly Luminescent Cesium Lead Halide Nanowires through Anion-Exchange Reactions. *J. Am. Chem. Soc.* **2016**, *138*, 7236−7239.
(28) Schmidt, L. C.; Pertegás, A.; González-Carrero, S.; Malinkiewicz, O.; Agouram, S.; Espallargas, G. M.; Bolink, H. J.; Galian, R. E.; Pérez-Prieto, J. Nontemplate Synthesis of $CH_3NH_3PbBr_3$ Perovskite Nanoparticles. *J. Am. Chem. Soc.* **2014**, *136*, 850−853.
(29) Huang, H.; Zhao, F.; Liu, L.; Zhang, F.; Wu, X.-g.; Shi, L.; Zou, B.; Pei, Q.; Zhong, H. Emulsion Synthesis of Size-Tunable $CH_3NH_3PbBr_3$ Quantum Dots: An Alternative Route toward Efficient Light-Emitting Diodes. *ACS Appl. Mater. Interfaces* **2015**, *7*, 28128−28133.
(30) Tong, Y.; Bladt, E.; Aygüler, M. F.; Manzi, A.; Milowska, K. Z.; Hintermayr, V. A.; Docampo, P.; Bals, S.; Urban, A. S.; Polavarapu, L.; Feldmann, J. Highly Luminescent Cesium Lead Halide Perovskite Nanocrystals with Tunable Composition and Thickness by Ultrasonication. *Angew. Chem. Int. Ed.* **2016**, *55*, 13887−13892.
(31) Jang, D. M.; Kim, D. H.; Park, K.; Park, J.; Lee, J. W.; Song, J. K. Ultrasound Synthesis of Lead Halide Perovskite Nanocrystals. *J. Mater. Chem. C* **2016**, *4*, 10625−10629.
(32) Chen, M.; Zou, Y.; Wu, L.; Pan, Q.; Yang, D.; Hu, H.; Tan, Y.; Zhong, Q.; Xu, Y.; Liu, H.; Sun, B.; Zhang, Q. Solvothermal Synthesis of High-Quality All-Inorganic Cesium Lead Halide Perovskite Nanocrystals: From Nanocube to Ultrathin Nanowire. *Adv. Funct. Mater.* **2017**, *27*, 1701121.
(33) Lignos, I.; Stavrakis, S.; Nedelcu, G.; Protesescu, L.; deMello, A. J.; Kovalenko, M. V. Synthesis of Cesium Lead Halide Perovskite Nanocrystals in a Droplet-Based Microfluidic Platform: Fast Parametric Space Mapping. *Nano Lett.* **2016**, *16*, 1869−1877.
(34) Maceiczyk, R. M.; Dümbgen, K.; Lignos, I.; Protesescu, L.; Kovalenko, M. V.; deMello, A. J. Microfluidic Reactors Provide Preparative and Mechanistic Insights into the Synthesis of Formamidinium Lead Halide Perovskite Nanocrystals. *Chem. Mater* **2017**, *29*, 8433−8439.
(35) Lee, G.-J.; Park, E.-K.; Yang, S.-A.; Park, J.-J.; Bu, S.-D.; Lee, M.-K. Rapid and Direct Synthesis of Complex Perovskite Oxides through a Highly Energetic Planetary Milling. *Sci. Rep.* **2017**, *7*, 46241.
(36) El Ajjouri, Y.; Palazon, F.; Sessolo, M.; Bolink, H. J. Single-Source Vacuum Deposition of Mechanosynthesized Inorganic Halide Perovskites. *Chem. Mater.* **2018**, *30*, 7423−7427.
(37) Protesescu, L.; Yakunin, S.; Nazarenko, O.; Dirin, D. N.; Kovalenko, M. V. Low-Cost Synthesis of Highly Luminescent Colloidal Lead Halide Perovskite Nanocrystals by Wet Ball Milling. *ACS Appl. Nano Mater.* **2018**, *1*, 1300−1308.
(38) Chen, D.; Chen, X.; Wan, Z.; Fang, G. Full-Spectral Fine-Tuning Visible Emissions from Cation Hybrid $Cs_{1-m}FA_mPbX_3$ (X=Cl, Br, and I, $0 \leq m \leq 1$) Quantum Dots. *ACS Appl. Mater. Interfaces* **2017**, *9*, 20671−20678.
(39) Nedelcu, G.; Protesescu, L.; Yakunin, S.; Bodnarchuk, M. I.; Grotevent, M. J.; Kovalenko, M. V. Fast Anion-Exchange in Highly Luminescent Nanocrystals of Cesium Lead Halide Perovskites ($CsPbX_3$, X =Cl, Br, I). *Nano Lett.* **2015**, *15*, 5635−5640.
(40) Levchuk, I.; Herre, P.; Brandl, M.; Osvet, A.; Hock, R.; Peukert, W.; Schweizer, P.; Spiecker, E.; Batentschuk, M.; Brabec, C. J. Ligand-Assisted Thickness Tailoring of Highly Luminescent Colloidal $CH_3NH_3PX_3$ (X=Br and I) Perovskite Nanoplatelets. *Chem. Commun.* **2017**, *53*, 244−247.
(41) He, J.; Vasenko, A. S.; Long, R.; Prezhdo, O. V. Halide Composition Controls Electron-Hole Recombination in Cesium-Lead Halide Perovskite Quantum Dots: A Time Domain Ab Initio Study. *J. Phys. Chem. Lett.* **2018**, *9*, 1872−1879.
(42) Hintermayr, V. A.; Richter, A. F.; Ehrat, F.; Döblinger, M.; Vanderlinden, W.; Sichert, J. A.; Tong, Y.; Polavarapu, L.; Feldmann, J.; Urban, A. S. Tuning the Optical Properties of Perovskite Nanoplatelets through Composition and Thickness by Ligand-Assisted Exfoliation. *Adv. Mater.* **2016**, *28*, 9478−9485.
(43) Xu, W.; Li, F.; Cai, Z.; Wang, Y.; Luo, F.; Chen, X. An Ultrasensitive and Reversible Fluorescence Sensor of Humidity Using Perovskite $CH_3NH_3PbBr_3$. *J. Mater. Chem. C* **2016**, *4*, 9651−9655.
(44) Akkerman, Q. A.; D'Innocenzo, V.; Accornero, S.; Scarpellini, A.; Petrozza, A.; Prato, M.; Manna, L. Tuning the Optical Properties of Cesium Lead Halide Perovskite Nanocrystals by Anion Exchange Reactions. *J. Am. Chem. Soc.* **2015**, *137*, 10276−10281.
(45) Zhang, F.; Huang, S.; Wang, P.; Chen, X.; Zhao, S.; Dong, Y.; Zhong, H. Colloidal Synthesis of Air-Stable $CH_3NH_3PbI_3$ Quantum Dots by Gaining Chemical Insight into the Solvent Effects. *Chem. Mater.* **2017**, *29*, 3793−3799.
(46) Dastidar, S.; Egger, D. A.; Tan, L. Z.; Cromer, S. B.; Dillon, A. D.; Liu, S.; Kronik, L.; Rappe, A. M.; Fafarman, A. T. High Chloride Doping Levels Stabilize the Perovskite Phase of Cesium Lead Iodide. *Nano Lett.* **2016**, *16*, 3563−3570.
(47) Brgoch, J.; Lehner, A. J.; Chabinyc, M.; Seshadri, R. Ab Initio Calculations of Band Gaps and Absolute Band Positions of Polymorphs of $RbPbI_3$ and $CsPbI_3$: Implications for Main-Group Halide Perovskite Photovoltaics. *J. Phys. Chem. C* **2014**, *118*, 27721−27727.
(48) Swarnkar, A.; Marshall, A. R.; Sanehira, E. M.; Chernomordik, B. D.; Moore, D. T.; Christians, J. A.; Chakrabarti, T.; Luther, J. M. Quantum Dot−Induced Phase Stabilization of α-$CsPbI_3$ Perovskite for High-Efficiency Photovoltaics. *Science* **2016**, *354*, 92−95.
(49) Chen, D.; Fang, G.; Chen, X. Silica-Coated Mn-Doped $CsPb(Cl/Br)_3$ Inorganic Perovskite Quantum Dots: Exciton-to-Mn Energy Transfer and Blue-Excitable Solid-State Lighting. *ACS Appl. Mater. Interfaces* **2017**, *9*, 40477−40487.
(50) Chen, D.; Zhou, S.; Fang, G.; Chen, X.; Zhong, J. Fast Room-Temperature Cation Exchange Synthesis of Mn-Doped $CsPbCl_3$ Nanocrystals Driven by Dynamic Halogen Exchange. *ACS Appl. Mater. Interfaces* **2018**, *10*, 39872−39878.
(51) Huang, H.; Chen, B.; Wang, Z.; Hung, T. F.; Susha, A. S.; Zhong, H.; Rogach, A. L. Water Resistant $CsPbX_3$ Nanocrystals Coated with Polyhedral Oligomeric Silsesquioxane and Their Use as Solid State Luminophores in All-Perovskite White Light-Emitting Devices. *Chem. Sci.* **2016**, *7*, 5699−5703.
(52) Zhou, Q.; Bai, Z.; Lu, W.-g.; Wang, Y.; Zou, B.; Zhong, H. In Situ Fabrication of Halide Perovskite Nanocrystal-Embedded Polymer Composite Films with Enhanced Photoluminescence for Display Backlights. *Adv. Mater.* **2016**, *28*, 9163−9168.
(53) Sun, C.; Zhang, Y.; Ruan, C.; Yin, C.; Wang, X.; Wang, Y.; Yu, W. W. Efficient and Stable White LEDs with Silica-Coated Inorganic Perovskite Quantum Dots. *Adv. Mater.* **2016**, *28*, 10088−10094.

DOI: 10.1021/acsami.8b19002
ACS Appl. Mater. Interfaces 2019, 11, 10059−10067